Characterization of Silver Image Formation in a Silver Behenate Photothermographic Imaging Element Using X-Ray Diffraction Techniques

Thomas N. Blanton*, Mark Lelental and Craig L. Barnes
Eastman Kodak Company, Research & Development Laboratories, Rochester, New York, USA

The quantitative assessment of silver development efficiency and covering power in silver based imaging elements requires an accurate determination of the coverage of silver metal (Ag(0)) formed as a result of post-exposure image development. The thermographic and photothermographic imaging processes do not incorporate a silver source removal-fixing step. Therefore, it has been necessary to develop an analytical technique capable of providing a quantitative determination of the Ag(0) coverage in the presence of silver salts and complexes. An X-ray diffraction method has been developed that is based on the correlation between silver metal diffraction peak area intensity and silver metal coverage present in the final image area. It has been demonstrated that this methodology may be used for the assessment of the development efficiency, covering power, and quantum efficiency in photothermographic, silver behenate based, imaging elements. The use of X-ray diffraction techniques has been extended to characterization of crystallinity, morphology, and crystallite size of micro- and nano-silver behenate particulates.

Journal of Imaging Science and Technology 49: 356–364 (2005)

Introduction

Silver based photothermographic (PTG) imaging systems have been explored and manufactured by the photographic industry for more than 30 years. The primary use of this technology has been focused on black and white microfilm, medical diagnostic laser printer output media, thermal printing, and graphic arts applications. During this period, a high degree of understanding of the chemistry and imaging mechanisms governing the performance of these photographic elements has been achieved. An extensive review of the present state of knowledge of PTG systems was recently published by Cowdery–Corvan and Whitcomb[1] and Strijckers.[2] In the last five years, the dynamic growth of the use of the silver carboxylate (behenate)-based PTG materials has been linked to the introduction and wide acceptance of photothermographic laser printers for medical diagnostic applications. It is expected that future growth will be fueled by the medical imaging industry's migration to digital modalities as X-ray imaging moves from screen-film combinations to computed radiography/digital radiography (CR/DR), magnetic resonance imaging (MRI), etc. The wide acceptance of the PTG products is primarily due to the elimination of the wet processing step used in conventional film systems by the incorporation of the heat-sensitive development chemistry in the imaging layer.

The typical photothermographic process is outlined in Fig. 1. The photographic response of the PTG elements is impacted by a number of factors, including efficiency of silver latent image formation, minimum size of the latent image site required for the initiation of the silver metal-forming redox amplification process, amplification factor, development efficiency, and covering power of the image silver.

In the traditional, wet processed black and white photographic silver halide products, the amount (coverage) of the image-forming silver metal in the developed film or paper can readily be determined using commonly known analytical techniques such as X-ray fluorescence spectroscopy (XRF). The fixing step in the traditional process leads to the removal of undeveloped silver halide. Therefore, the silver XRF signal can be attributed to the developed image silver. However, in heat processed photothermographic elements several silver containing species can be present and all will contribute to the silver XRF signal. These species include silver halide(s), silver carboxylate (behenate), and silver metal. In the absence of the fixing step in PTG elements, it is necessary to use a quantitative analytical technique capable of determining silver metal coverage in the presence of the various silver containing species.

It was an object of this work to develop an X-ray diffraction (XRD) method for the quantitative determination of the silver metal in the unexposed, exposed, and thermally processed photothermographic elements and to apply the XRD data to assess the macroscopic development efficiency, covering power, and macroscopic quantum efficiency of image silver. It is expected that quantification of these parameters will provide a better understanding of factors that determine photographic responses of PTG elements as compared with traditional black-and-white film systems.

Original manuscript received August 23, 2004

Corresponding Author: Thomas Blanton, thomas.blanton@kodak.com

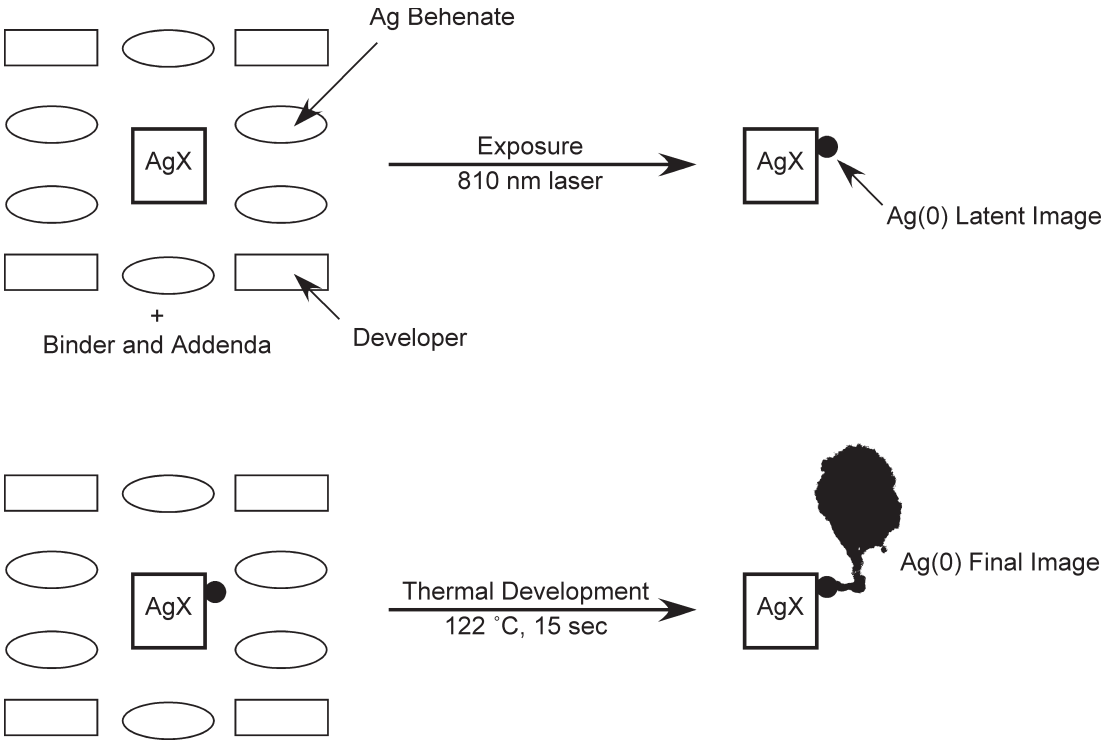

Figure 1. Two-step photothermographic process for an 810 nm sensitized aqueous dispersed PTG film. Step 1 is the exposure, step 2 is a typical thermal processing resulting in Ag(0) formation.

TABLE I. Unit Cell Parameters for Ag-Containing Phases Utilized in Photothermographic Imaging Elements

Phase	Bravais Lattice	Space Group	Unit Cell Lengths (Å)	Unit Cell Angles (°)
Ag(0)	Face-centered cubic	Fm-3m	4.0859	90
AgBr	Face-centered cubic	Fm-3m	5.7748	90
AgBehenate	Triclinic	P1 or P-1	4.71/4.15/60.30	104.5/93.2/75.6

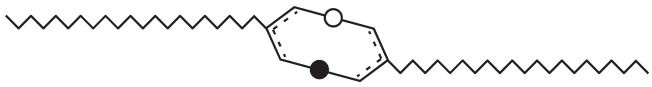

Figure 2. Head-to-head dimer structure of silver behenate.

In silver behenate based photothermographic elements, the three silver containing phases of silver metal (Ag(0)), silver behenate (AgBeh), and silver halide (AgX) have differing crystal structures. Unit cell data for these three materials are shown in Table I.

The crystal structures of Ag(0) and AgBr are well known. The crystal structure for silver behenate has not been reported. The unit cell data reported in Table I for AgBeh are based on powder X-ray diffraction measurements using a synchrotron radiation source. Although we have yet to complete crystal structure determination, we can say that AgBeh it is analogous to the structures reported by Vand and co-workers[3] for Ag fatty acid derivatives with carbon chains of C_{10} to C_{16} and silver stearate as reported by Whitcomb et al.[4] Silver behenate is a crystalline, long chain silver carboxylate, $CH_3(CH_2)_{20}COOAg$, that crystallizes as a dimer in a head-to-head configuration (Fig. 2). The morphology of AgBeh is typically plate-like, with the (00l) lattice plane parallel to the plate surface.[5]

X-ray powder diffraction (XRD) is the principle analytical technique used for phase identification of crystalline materials. The uniqueness of the crystal structures and unit-cell parameters for Ag(0), AgX, and AgBeh result in XRD patterns (Fig. 3) that provide a fingerprint for these phases. One or multiple peaks from a phase can be used to assess the presence or absence of a phase, as well as how much of that phase is present. In the diffractometer scan range shown in Fig. 3, one can observe the (111) peak for Ag(0) at 38.15 °2θ, the (200) peak for AgBr at 30.89 °2θ, and a series of (00l) diffraction peaks at low 2θ for AgBeh. In Fig. 4, the diffraction pattern of a photothermographic element coated on poly(ethylene terephthalate), PET, support is shown for a neat unprocessed sample (Fig. 4(a)) and a maximum optical density (Dmax) thermally processed sample (Fig. 4(b)). The unprocessed film sample is found to be comprised of AgBeh and AgBr, along with the PET support. The processed film sample shows that AgBr is still present, but the AgBeh has been reduced and has been converted to Ag(0), as demonstrated by the presence of the Ag(0) (111) peak at 38.15 °2θ. The ability to identify all three silver phases by XRD allows for analysis of photothermographic films over a variety of exposure levels and allows for quantification of silver metal development. Although a technique such as X-ray fluorescence (XRF) can determine total silver coverage in a photothermographic film, XRF is unable to differentiate between the phases that contain Ag, either as a metal or cation. The quantification of silver metal development using XRD provides a means to determine the development efficiency, covering powder, and macroscopic quantum efficiency in photothermographic, silver behenate based imaging elements.

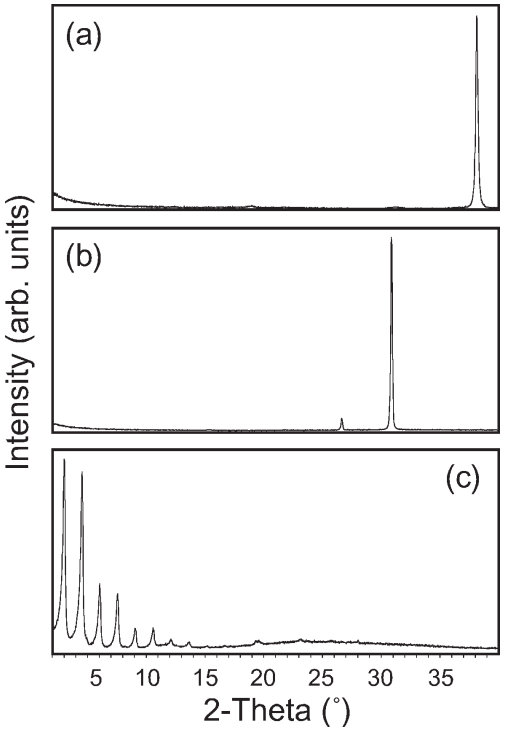

Figure 3. X-ray diffraction patterns for (a) Ag(0), (b) AgBr, and (c) AgBehenate.

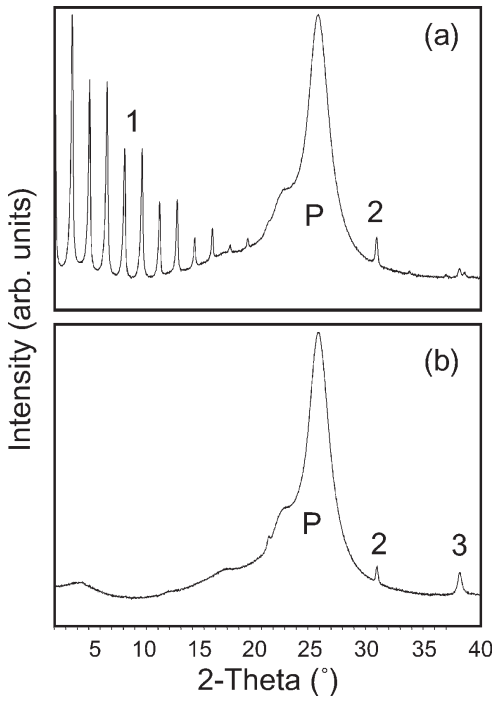

Figure 4. X-ray diffraction patterns for (a) PTG film, unexposed and unprocessed and (b) Dmax PTG film, exposed for maximum optical density and processed. (1 = AgBeh, 2 = AgBr, 3 = Ag(0), P = PET)

Experimental

An aqueous silver behenate based photothermographic element containing a microparticulate AgBeh aqueous dispersion was formulated and coated on a blue polyester film support as described by Lelental et al.[6] The PTG layer (19.2 μm thickness) comprised silver carboxylate, 57 nm edge length cubic silver halide grains, 683 nm infrared (IR) sensitizing dye, developer, toner, antifoggant, and binder. The coated imaging elements were exposed using a 683 nm diode laser sensitometer followed by heat processing at 121°C for 5 s to produce a developed sensitometric strip (21 steps) with an optical density range from D = 0.2 (Dmin) to D > 3.5 (Dmax).

An analogous aqueous silver behenate based photothermographic element containing a nanoparticulate-AgBeh aqueous dispersion prepared by attrition media milling[7] of the above cited microparticulate dispersion was formulated, coated (19.2 μm thickness) on a blue polyester film support, exposed, and processed as described above.

A third aqueous silver behenate based photothermographic element containing a nanoparticulate-AgBeh aqueous dispersion, prepared by controlled precipitation in the presence of a surface modifier and 810 nm IR sensitized, 57 nm edge length cubic silver halide grains, was formulated and coated (19.2 μm thickness) on a blue polyester film support.[8] These coated imaging elements were exposed using an 810 nm diode laser sensitometer followed by heat processing at 122°C for 9 s to produce a developed sensitometric strip with an optical density range from D = 0.2 (Dmin) to D > 3.5 (Dmax).

A commercially available solvent-based silver behenate photothermographic element, Kodak DryView™ Film, was formulated and coated (20.3 μm thickness) on a blue polyester film support. The PTG layer comprised silver carboxylate, 55 nm edge length cubic silver halide, 810 nm IR sensitizing dye, developer, toner, antifoggant, and binder. The coated imaging elements were exposed using a 810 nm diode laser sensitometer followed by heat processing at 121°C for 5 s to produce a developed sensitometric strip (21 steps) with an optical density range from D = 0.2 (Dmin) to D > 3.5 (Dmax).

X-ray diffraction measurements were made using a Rigaku Bragg–Brentano diffractometer equipped with a copper rotating anode, diffracted beam monochromator, and scintillation detector. All diffraction data were collected at ambient temperature. Samples were analyzed after actinic radiation exposure and thermal processing, as coatings on poly(ethylene terephthalate) (PET) support.

Phase identification of Ag(0), AgX, and AgBeh was confirmed using the powder diffraction file (PDF)[9] for Ag(0) and AgBr and an in-house reference pattern for AgBeh.

Crystallite size was determined using the Scherrer technique[10] with National Institute of Standards and Technology (NIST) Silicon 640b being used as the instrument profile standard. A value of 0.9 was used for the shape factor k in the Scherrer equation.

Silver development efficiency was determined using a calibration curve based on coatings of silver metal colloidal dispersions on PET. To ensure that Ag(0) morphology did not affect the results of the calibration curve, calibration coatings comprised of spherical Ag(0) (Fig. 5(a)) or filament Ag(0) (Fig. 5(b)) particles were used. Silver coverage of the Ag metal standards was determined using XRF, followed by XRD measurement of the (111) Ag(0) diffraction peak area (one analysis for each standard) for a series of standards with a Ag coverage range of 0.127 – 2.011 g/m^2. The XRD versus XRF calibration curve is shown in Fig. 6. These data indicate that the morphology of the Ag(0) colloidal particles is not

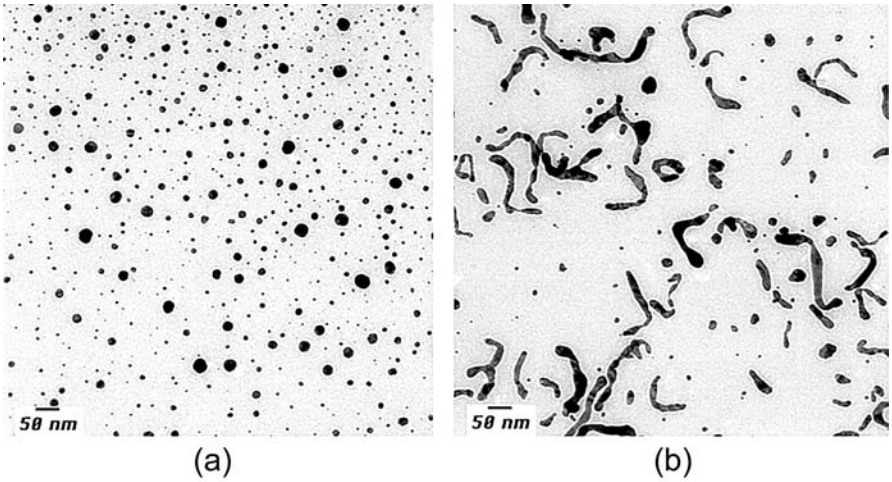

Figure 5. Scanning electron micrographs of (a) spherical, and (b) filamentary silver metal particles coated on polyester support.

a significant factor in XRD analysis of Ag(0) content in photothermographic coatings. The r^2 value of 0.998 is an indication that the XRD method is suitable to quantitate the Ag metal coverage in photothermographic films. Quantitative determination of silver as AgBr was carried out by XRD using a series of calibration films comprised 60 nm cubic AgBr grains coated on PET with a Ag coverage range of 0.054 – 1.076 g/m^2, as determined by XRF. XRD data were collected by measuring the (200) AgBr peak area for each film sample. A calibration curve similar to Fig. 6 was established for Ag as silver halide with an r^2 value of 0.991. Since an X-ray source used in XRD data collection loses intensity with time, it is necessary to establish a new calibration curve by re-running the standards by XRD prior to data collection for a new group of processed PTG films.

A method for assessing AgBeh crystallinity was proposed by Geuens and Vanwelkenhuysen.[11] This method utilizes the measurement and summation of six low-angle AgBeh diffraction peak height intensities and the measurement and summation of three NIST 1976 α-Al_2O_3 diffraction peak height intensities. Next, the calculation of a ratio of AgBeh/α-Al_2O_3, normalized to Ag coverage determined by XRF, is carried out to provide an index related to crystallinity. Crystallinity, however, is only one of a number of characteristics that impact AgBeh peak intensity. It has been shown through rocking-curve analysis that tilting an oriented sample of AgBeh 0.3° can result in a 50% loss in AgBeh peak intensity.[12] Therefore, the method described above provides information representing a crystallinity-orientation index. This approach was utilized to assess the effect of AgBeh morphology on the observed XRD peak intensity data.

Results and Discussion

Effect of Precipitation Method on Silver Behenate Morphology

Scanning electron microscopy (SEM) micrographs of microparticulate AgBeh and nanoparticulate AgBeh from aqueous formulations are shown in Figs. 7(a) and 7(b), respectively. Microparticulate AgBeh comprises plate-like particles with a nominal size of 0.5 – 2 μm (about 0.1 µm thickness), whereas the nanoparticulate AgBeh is spherical with a narrow size distribution of about 0.15 µm. It has been observed that media-milled AgBeh nanoparticles exhibit a higher degree of sphere-like morphology than nanoparticulates prepared by controlled precipitation. The effect of particle morphology on XRD analysis of AgBeh is demonstrated in Fig. 8 where the diffraction peak profile for nano AgBeh exhibits diffraction peak line broadening, which is due to smaller crystallite size when compared to microparticulate AgBeh. Crystallite size data for micro- and nanoparticulate AgBeh are shown in Table II.

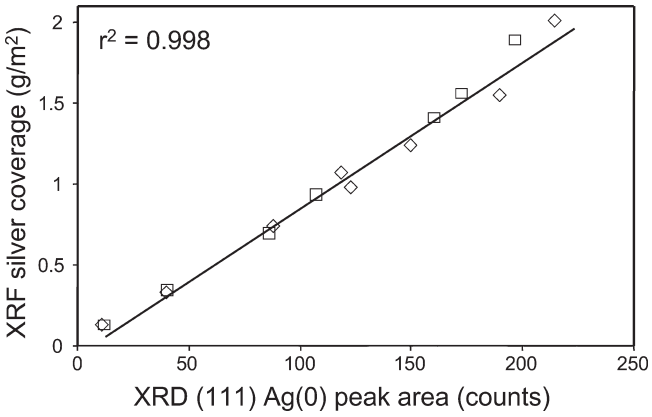

Figure 6. Silver calibration curve for determination of Ag(0) coverage using (◇) spherical and (□) filamentary silver metal film coatings. Coverage values certified by X-ray fluorescence.

According to the data in Table II, the crystallite size is found to be smaller than the grain size estimates from the SEM images shown in Figs. 7(a) and 7(b), respectively. This effect is an indication that the AgBeh particles may comprise smaller grains or contain a large population of defects, such as dislocations and/or grain boundaries that are registered by XRD as perturbations in the AgBeh grain. These perturbations lead to discontinuities in X-ray scattering, resulting in broadening of the XRD peak profile and a lower calculated crystallite size when compared to the particle size. Any preferred orientation of the AgBeh grains would not be expected to bias the crystallite size values, as the Scherrer equation is dependent upon the peak width and not the peak height.

The effect of AgBeh morphology on the peak heights of the AgBeh XRD patterns can be seen in Fig. 9. Although the specimens that were analyzed to generate the data

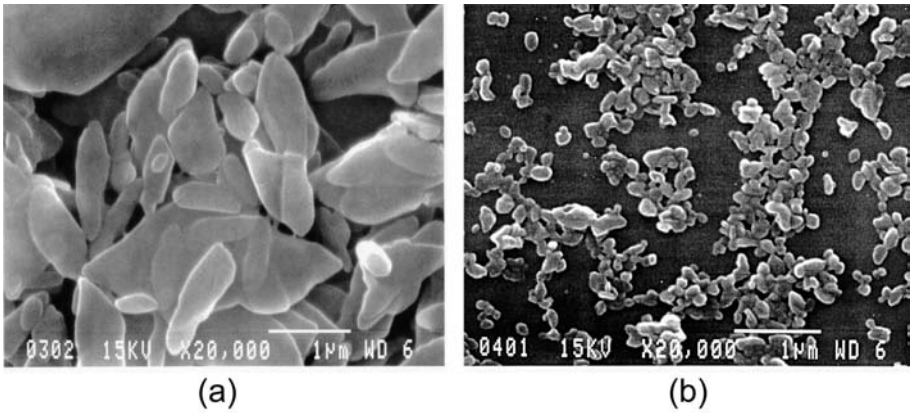

Figure 7. Transmission electron micrographs of aqueous dispersed (a) micro, and (b) nanoparticulate AgBeh.

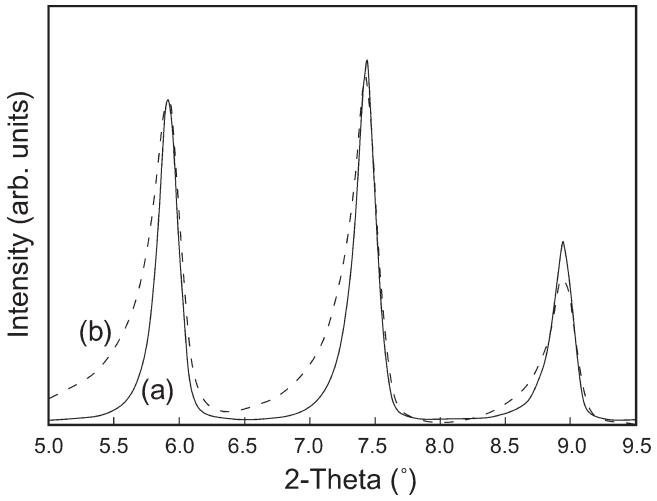

Figure 8. Selected range X-ray diffraction patterns of aqueous dispersed (a) micro (solid line), and (b) nanoparticulate (dashed line) AgBehenate. Peak heights normalized to the (004) diffraction peak at ~6 °2 .

in Fig. 9 have the same AgBeh coverage, significant differences in AgBeh peak height intensity are observed. The plate-like nature of the microparticulate AgBeh leads to the preferred alignment of the (00l) AgBeh lattice planes parallel to the substrate surface.[12] The effect this preferred orientation has on the XRD pattern is an enhancement of the intensity of the (00l) diffraction peaks (Fig. 9(a)) in comparison to a sample comprising randomly oriented particles. In contrast to the XRD pattern resulting from microparticulate AgBeh films, the analogous nanoparticulate AgBeh samples exhibit diffraction patterns with significantly reduced (00l) diffraction peak intensity. The reduced nanoparticulate diffraction peak intensity can be attributed to a more spherical like particle morphology as shown in Fig. 7(b). A spherical morphology, in general, tends to favor a random alignment of lattice planes for particulate dispersions coated on a substrate.[13]

Furthermore, comparison of the X-ray diffraction patterns of films coated with nanoparticulate AgBeh prepared using either controlled precipitation[8] (Fig. 9(b)) or media milling[7] (Fig. 9(c)) indicates that (00l) diffraction peaks are lowest in intensity for the more spherical nanoparticulate media milled AgBeh. A quantitative assessment of orientation is presented in

TABLE II. Silver Behenate Crystallite Size as a Function of Particle Morphology

Aqueous AgBeh Particle Type	(00l) Scherrer Crystallite Size (Å)
Micro	1000
Nano–media milling	290
Nano–controlled precipitation	290

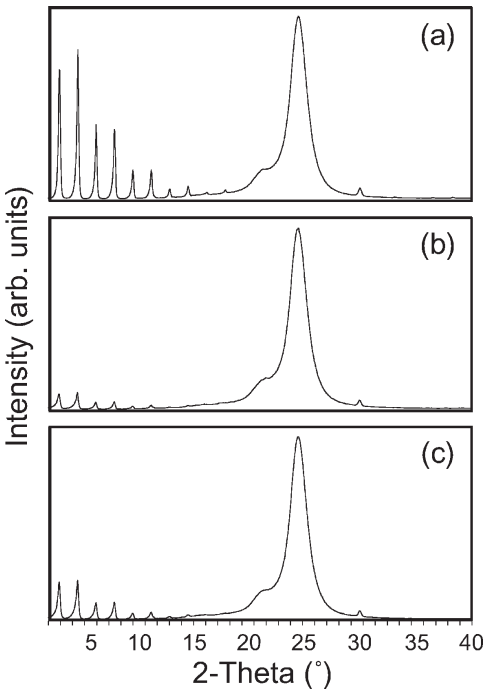

Figure 9. X-ray diffraction patterns from films of aqueous dispersed (a) micro, (b) controlled precipitation nano, and (c) attrition-milled nano AgBehenate coated on PET support.

Table III. Crystallinity orientation index values[11] confirm the effect of particle morphology on the preferred orientation of AgBeh particles in coated films.

A value of 3.21 for microparticulate AgBeh is an indication that large plate-like grains exhibit a higher propensity for alignment of (00l) lattice planes parallel to the film support. Furthermore, the lower values of crystallinity orientation index observed for nanoparticulate materials are indicative of a reduced degree

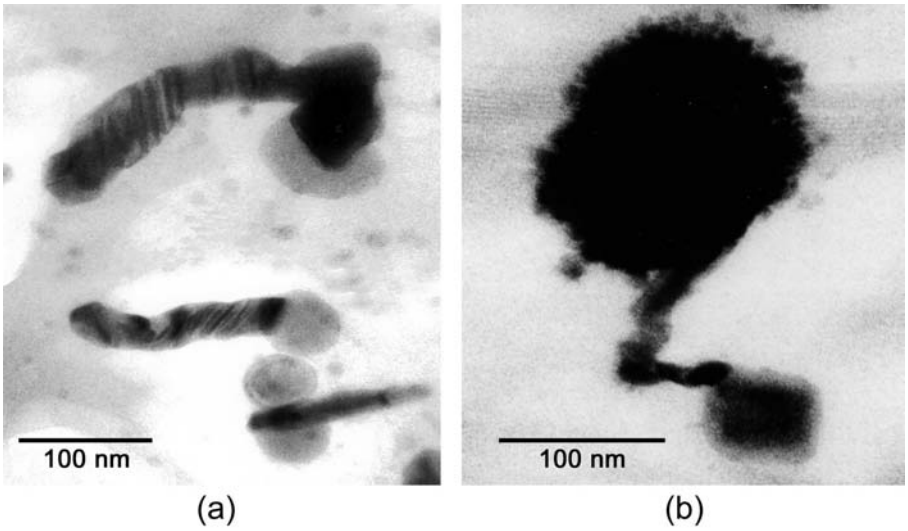

Figure 10. Transmission electron micrographs of exposed and thermally processed PTG film samples coated with (a) aqueous, and (b) DryView solvent-dispersed silver behenate. A filament forms off the AgBr grain in (a), and a filament followed by a cluster of dendrites forms off the AgBr grain in (b).

Table III. Crystallinity-Orientation Index of Coated Aqueous Precipitated AgBeh Particles

AgBeh particle type	Crystallinity-orientation index
Microparticulate	3.21
Nanoparticulate–controlled precipitation	0.88
Nanoparticulate–media milled	0.33

of alignment of (00l) lattice planes parallel to the film support.

Effect of PTG Image Silver Morphology on X-ray Diffraction Peak Profiles

Transmission electron microscopy (TEM) micrographs of image silver formed in aqueous nanoparticulate PTG film of this study (Fig. 10(a)) and in solvent-based Kodak DryView™ Film (Fig. 10(b)) display significant differences in the silver morphology. The image silver in the nanoparticulate film exhibits a filamentary morphology, whereas in the case of the image silver in the DryView film, both filamentary and dendroic morphologies are observed. These different morphologies can be attributed to the significant differences in the formulation of these two photothermographic films. The effect of the silver morphology on X-ray diffraction data can be observed in Fig. 11. The peak shape of the (111) Ag(0) diffraction peak for the nanoparticulate sample (Fig. 11(a)) is uniform and has no extended peak tails. Profile fitting of this pattern can be accomplished using a single pseudo-Voight peak.[14] The extended tailing for the (111) Ag(0) peak (Fig. 11(b)) observed in the DryView film sample diffraction pattern requires two pseudo-Voight diffraction peaks to correctly profile fit the diffraction pattern to determine the peak area. The tails observed in Fig. 11(b) are due to the small crystallite size of the silver dendrites, comprising an assembly of small spherical particles. The narrow component of the diffraction pattern in Fig. 11(b) is the result of diffraction from the larger silver filaments. With this understanding of the origin of the (111) Ag(0) diffraction peak shape, Ag(0) coverage determination by XRD can be carried out independent of image silver morphology.

XRD Determination of Ag^o Coverage

Selected-range X-ray diffraction patterns for heat processed DryView photothermographic film samples are shown in Fig. 12 for AgBeh and Fig. 13 for Ag metal. The data in Fig. 12 indicate a loss in AgBeh diffraction peak intensity consistent with the reduction of AgBeh during the photothermographic development process. Comparing the peak-height intensities in Fig. 12 for the unexposed (Dmin) step to Step 7 of the sensitometric step, there is a 37% loss in AgBeh peak-height intensity. Conversely, the intensity of the (111) Ag(0) peak for Step 7 in Fig. 13, does not correspond to 37% of the total Ag in the sensitometric strip (taking into account the presence of AgBr), as measured by XRF. This observation is an indication that the loss of AgBeh, as observed by XRD, is not an accurate quantitative measure of Ag(0) formation. This point is further supported with the observation that at Step 19, no AgBeh is observed by XRD, whereas the Ag(0) diffraction peak continues to increase in intensity from Step 19 to 21. Kinetic studies[15] of AgBeh reduction and Ag(0) development have shown that the AgBeh reduction process follows second-order kinetics, which suggest that an unidentified intermediate phase is formed before final reduction to Ag(0). This observation is consistent with results reported by Usanov[16] and Maekawa[17] where thermal development begins with phthalic acid reacting with AgBeh, resulting in a loss of crystalline silver behenate. The overall reaction scheme eventually is completed with the reduction of silver ion to produce Ag(0).

Quantitative XRD Ag(0) data from a selected PTG sensitometric strip are shown in Table IV. These data were obtained from integration of the Ag(0) (111) diffraction peak and conversion to Ag(0) coverage using the calibration curve generated as described above.

Development Efficiency and Covering Powder

Two PTG films, Kodak DryView and one formulated with aqueous nanoparticulate AgBeh, prepared by controlled precipitation, were compared for development efficiency and covering power. The first step required determination of total silver coverage using X-ray fluorescence. Total silver (Ag(0) + AgX + AgBeh) was found to be 1.957

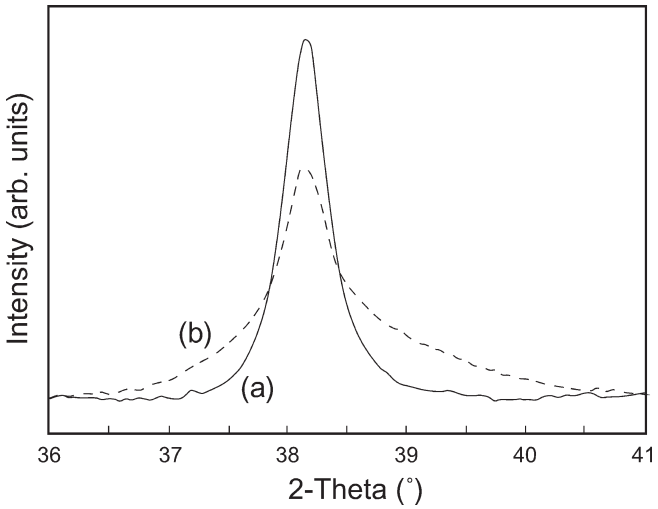

Figure 11. Selected range X-ray diffraction pattern for PTG exposed and processed films, (111) Ag(0) peak. Coated with (a) aqueous (solid line) and (b) DryView (dashed line) solvent-dispersed silver behenate.

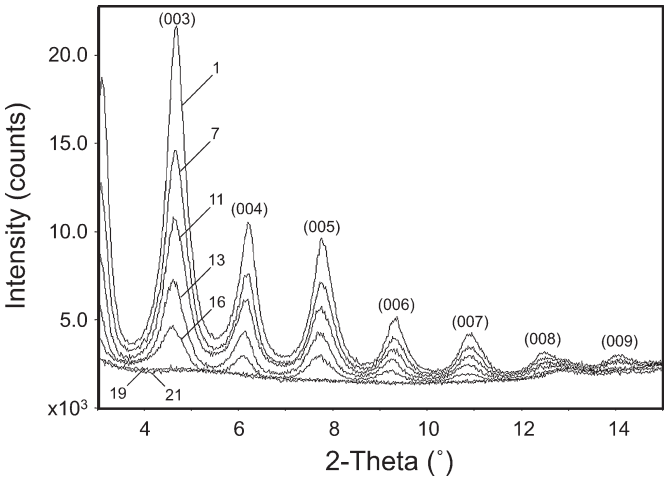

Figure 12. AgBehenate-selected range X-ray diffraction patterns, (003) – (009) AgBeh peaks, for PTG-exposed and processed Dry View film. Number refers to step position on sensitometric strip (Dmin = Step1, Dmax = Step 21).

and 2.040 g/m² for DryView and nanoparticulate AgBeh films, respectively.

Silver development efficiency (SDE) is defined in this study as follows:

$$\mathrm{SDE}(\%) = \frac{\text{Developed Ag(0) Coverage}}{\text{Total Ag Coverage } [\mathrm{Ag(0) + AgX + AgBeh}]} \times 100 \quad (1)$$

where the percent SDE is the ratio of the developed silver coverage (determined by XRD) to the total silver, as measured using XRF. Since the silver as AgBr accounts for 0.269 g/m² silver in both PTG films and the XRD data indicate no change of the (200) AgBr peak intensity after thermal processing, the maximum achievable SDE for DryView film would be 86.3% and for aqueous nanoparticulate AgBeh film it would be 86.8%. Silver coverage, SDE, and net OD values (measured optical density – Dmin optical density (0.20)) for both films, after exposure and processing, are shown in Table V.

The relationship between optical density (OD) and silver development efficiency for DryView and nanoparticulate aqueous AgBeh PTG films is shown in Fig. 14. In the case of DryView film, the upper optical density point (OD = 3.525, Step 20) corresponds to a development efficiency approaching greater than 80%. An OD of 2.728 (Step 20) for the nanoparticulate aqueous AgBeh PTG film is observed at a development efficiency of about 60%. Various factors may contribute to these different development efficiencies. They include differences in intrinsic photosensitivity, potential depletion of the component(s) essential to the propagation of the silver reduction process, and differences in the effective size of "sphere of influence," etc.[18,19] Furthermore, the upper density points achieved in this work may not represent the maximum that is attainable under optimum exposure and processing conditions. The elucidation of the mechanisms limiting image silver formation efficiencies in the PTG elements would require more extensive experimental effort.

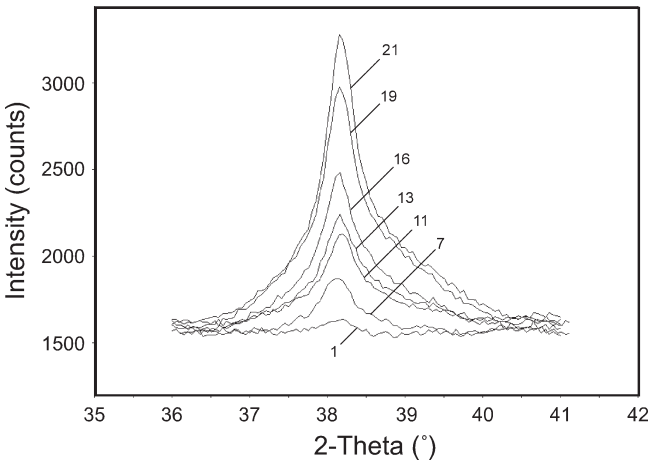

Figure 13. Silver metal selected range X-ray diffraction patterns, (111) Ag(0) peak, for PTG exposed and processed Dry View film. Number refers to step position on sensitometric strip (Dmin = Step1, Dmax = Step 21).

TABLE IV. Image Silver Coverage and Optical Density for an Exposed/Heat Processed KODAK DryView PTG Film Strip*

PTM Step Number	Ag(0) Coverage g/m² from XRD	Optical Density
4	0.103	0.142
7	0.183	0.298
8	0.216	0.431
11	0.493	1.188
13	0.876	1.786
15	0.959	2.337
16	1.059	2.580
18	1.176	2.949

* total silver coverage by XRF: 2.038 g/m²; 0.269 g/m² Ag as AgBr (determined by XRD)

TABLE V. Silver Coverage, Silver-Development Efficiency, and Optical Density Values for KODAK DryView and nanoparticulate AgBeh PTG films

DryView				Nanoparticulate AgBeh, Controlled Precipitation			
Step	Silver Coverage (g/m²)	SDE (%)	Net OD	Step	Silver Coverage (g/m²)	SDE (%)	Net OD
8	0.030	1.53	0.075	7	0.183	8.97	0.098
10	0.156	7.97	0.274	8	0.216	10.59	0.231
12	0.450	22.99	0.898	11	0.493	24.17	0.888
14	1.083	55.34	2.059	13	0.876	42.94	1.586
16	1.421	72.61	2.981	15	0.959	47.01	2.137
18	1.483	75.78	3.340	16	1.059	51.91	2.380
19	1.563	79.87	3.446	18	1.176	57.65	2.749
20	1.434	73.28	3.525	20	1.202	58.92	2.728

TABLE VI. Covering Power of DryView and Nanoparticulate AgBeh PTG Films

DryView		Nanoparticulate AgBeh, Controlled		
Step	CP (m²/g)	Step	Precipitation	CP (m²/g)
8	2.50	7		0.54
10	1.76	8		1.07
12	2.00	11		2.00
14	1.90	13		1.81
16	2.10	15		2.23
18	2.25	16		2.25
19	2.20	18		2.34
20	2.46	20		2.27

The mass of silver per unit area divided by the optical density of a processed film is defined as the photometric equivalent, *PE*.[20] The reciprocal of the *PE* is termed covering power (CP) and is dependent upon the size, structure, and physical density of developed silver centers along with the method of optical density measurement.

$$CP = OD/M \quad (2)$$

where *OD* is optical density and *M* is Ag(0) coverage expressed in g/m² as measured by XRD.

Using data from Table V, the *CP* for DryView and nanoparticulate AgBeh PTG films is presented in Table VI, and a plot of Ag(0) coverage versus *OD* is shown in Fig. 15.

Farnell and Solman[21–24] extensively analyzed the factors affecting silver image covering power for the traditional black-and-white films, including the angle of light collection, exposure and degree of development, choice of binder, silver morphology, and image tone. According to Solman,[24] the maximum *CP* for filamentary image silver is about 1.8 m²/g, and maximum white light *CP* for neutral particulate silver deposit is estimated to be 5.0 m²/g. Therefore, the data shown in Table VI indicate that it is possible to achieve image silver covering power in the heat developed PTG films approaching values observed in traditional black and white films.

Macroscopic Quantum Efficiency

The quantification of the image silver coverage versus optical density relationship for the two PTG films examined in this work provides an opportunity for the assessment of the macroscopic quantum efficiency (*MQE*). The 810 nm *MQE* is defined in this work as the average number of image silver atoms formed per photon absorbed by the PTG film. The 810 nm laser-light absorption measurements[25] were carried out using a diode laser operated at ~50 mW power, and indicate that 1.2 and 5.0% of incident photons are absorbed by the DryView and aqueous nanoparticulate PTG films, respectively. The *MQE* values calculated for different net *OD* points of the sensitometric curve, using well-characterized laser exposure, measured fraction of incident photons absorbed. and image silver coverage XRD data, are shown in Fig. 16.

It is noteworthy that MQE values in the $10^4 - 10^5$ Ag atoms/absorbed photon range for the PTG elements comprising 57 nm edge length cubic AgBr grains[6] are not that different from the values expected for the

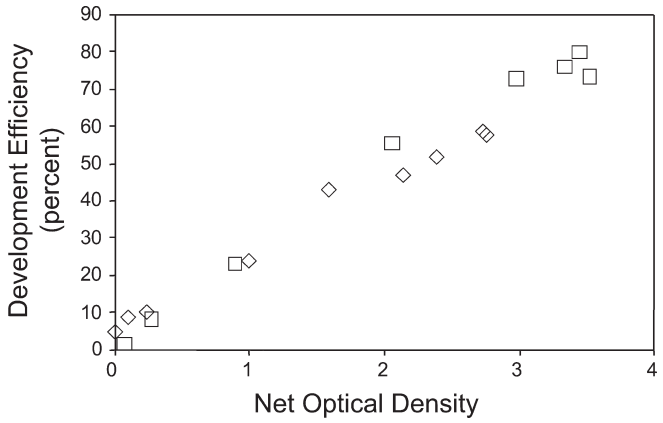

Figure 14. Plot of development efficiency verses net optical density for PTG exposed and processed films coated with (◇) aqueous and (□) DryView solvent dispersed silver behenate.

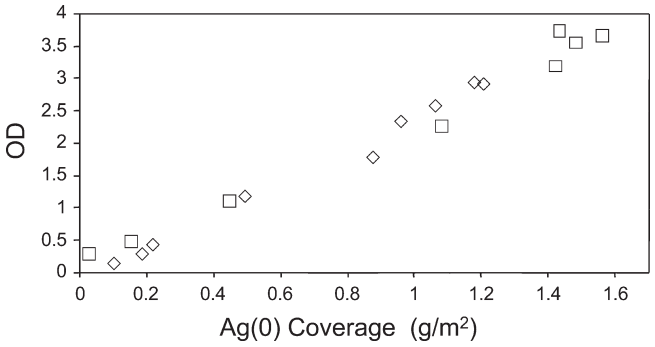

Figure 15. Plot of optical density versus Ag(0) coverage for PTG exposed and processed films coated with (◇) aqueous and (□) DryView solvent-dispersed silver behenate.

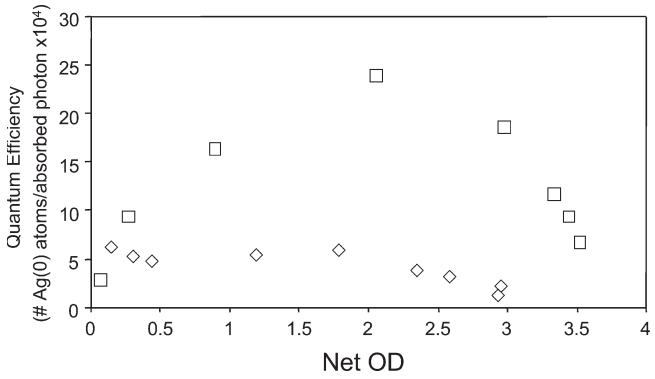

Figure 16. Plot of macroscopic quantum efficiency versus net optical density for PTG exposed and processed films coated with (◇) aqueous and (□) DryView solvent dispersed silver behenate.

traditional, black and white ~57 nm grain size AgBr films developed using traditional wet processing. This observation seems to indicate that in the case of some PTG films under certain experimental conditions, it is possible to achieve the efficiency of the latent image formation, developability of the latent image sites, and the amplification factors approaching those observed in fine grain traditional AgX-based films.

Conclusions

Quantitative X-ray diffraction methods for evaluating silver metal generated from thermal processing of photothermographic films were developed and allow for the determination of silver development efficiency, covering powder, and macroscopic quantum efficiency. Silver metal and silver behenate morphologies were found to have a significant effect on X-ray diffraction patterns.

Conventional precipitation methods result in microparticulate AgBeh grains, whereas attrition milling and controlled precipitation generate nanoparticulate AgBeh dispersions. Micro AgBeh was found to have a larger crystallite size and larger crystallinity-orientation index value when compared to nano AgBeh. Silver metal resulting from PTG processing can exhibit two morphologies, filamentary and dendroic. Filamentary particles give a narrow X-ray diffraction peak, while dendritic particles lead to extended tails in the silver diffraction pattern. (Aqueous dispersed PTG films showed one, and DryView solvent-dispersed PTG films showed two Ag(0) diffraction peak profiles). Having established the ability to measure accurately the peak area of the silver metal diffraction peaks, quantitative determination of Ag(0) coverage in PTG films using XRD was possible using a calibration curve based on X-ray fluorescence calibrated Ag(0) film standards. The silver metal coverage values were subsequently used to determine silver development efficiency, covering power, and macroscopic quantum efficiency.

The results presented in this article indicate that the photographic responses of the state-of-the-art PTG films formulated using fine grain AgX emulsion do not significantly differ from those typically observed in fine grain traditional black and white films.

Acknowledgment. We thank our colleagues at Eastman Kodak Company for their contributions to this study: Dr. Anne West for SEM micrographs, Dr. Sam Chen for TEM micrographs, Dr. Steven Kong for laser-light absorption measurements, Mr. Jim Wakely for PTG film preparation, and Dr. Dave Whitcomb and Dr. Lilia Burleva for their review of this study.

References

1. P. J. Cowdery-Corvan and D. R. Whitcomb, in "Photothermographic and Thermographic Imaging Materials", *Handbook of Imaging Materials*, A. Diamond and D. Weiss, Eds. (Marcel Dekker Inc., New York, 2002) pp. 473–529.
2. H. L. Strijckers, *J. Imaging Sci. and Technol.* ISSN: 1062-3701, **47**(2), 100 (2003).
3. V. Vand, A. Aitken and R. K. Cambell, *Acta. Cryst.* **2**, 398 (1949).
4. B. P. Tolochko, S. V. Chernov, S. G. Nikitenko, and D. R. Whitcomb, *Nucl. Instr. Meth. Phys. Res. (A)*, ISSN: 0168-9002, **405**, 428, (1998).
5. T. C. Huang, H. Toraya, T. N. Blanton, and Y. Wu, *J. Appl. Cryst.* ISSN: 0021-8898, **26**, 180, (1993).
6. M. Lelental, A. R. Pitt, D. A. Dickinson, J. L. Wakely, and P. J. Ghyzel, US Patent 6,391,537, Examples 2 and 4 (2002).
7. M. Lelental, A. R. Pitt, D. A. Dickinson, J. L. Wakely, and P. J. Ghyzel, US Patent 6,391,537, Examples 1 and 3 (2002).
8. M. Lelental, A. R. Pitt, D. A. Dickinson, J. L. Wakely, and P. J. Ghyzel, US Patent 6,391,537, Example 5 (2002).
9. Powder Diffraction File, International Center for Diffraction Data, 12 Campus Boulevard, Newtown Square, Pennsylvania, 19073-3273, USA. Ag(0) PDF 4-783, AgBr PDF 6-438.
10. B. D. Cullity, *Elements of X-ray Diffraction 2nd ed.*, (Addison-Wesley, Reading, Massachusetts, 1978) p. 102.
11. I. Geuens and I. Vanwelkenhuysen, *J. Imaging Sci. Technol.* ISSN: 1062-3701, **43**(6), 520 (1999).
12. T. N. Blanton, C. L. Barnes, and M. Lelental, *J. Appl. Cryst.* ISSN: 0021-8898, **33**, 172, (2000).
13. D. L. Bish and R. C. Reynolds, *Modern Powder Diffraction – Reviews in Mineralogy*, D. L. Bish and J. E. Post, Eds., (The Mineralogical Society of America, Washington, D.C., 1989), chap. 4, pp. 73–99.
14. S. A. Howard and K. D. Preston, *Modern Powder Diffraction – Reviews in Mineralogy*, D. L. Bish and J. E. Post Eds., (The Mineralogical Society of America, Washington, D.C., 1989), chap. 6, pp. 217–276.
15. T. Blanton, M. Lelental, S. Zdzieszynski, and S. Misture, *Adv. X-ray Anal.* ISSN: 0376-0308, **45**, 371 (2002).
16. Y. E. Usanov, T. B. Kolesova, M. Gulikova, L. P. Burleva, M. R. V. Sahyan, and D. R. Whitcomb, *J. Imaging Sci. Technol.* ISSN: 1062-3701, **43**, 545 (1999).
17. T. Maekawa, M. Yoshikane, H. Fujimura, and I. Toya, *J. Imaging Sci. Technol.* ISSN: 1062-3701, **45**, 365 (2001).
18. D. H. Klosteboer, in *Imaging Processes and Materials, Nebletters* 8th ed. J. Sturge, V. Walworth, and A. Shepp, Eds., (Van Nostrand-Reinhold, New York, 1989) pp. 279–291.
19. S. H. Kong, *J. Imaging Sci. Technol.* ISSN: 1062-3701, **43**, 509, (1999).
20. T. H. James, "The Rate of Development," *The Theory of the Photographic Process*, 4th ed., T. H. James. Ed. (MacMillan Publishing Co., New York, 1977), p. 405.
21. G. C. Farnell and L. R. Solman, *J. Photogr. Sci.* ISSN: 0022-3638, **18**, 94 (1970).
22. L. R. Solman, *J. Photogr. Sci.* ISSN: 0022-3638, **18**, 136 (1970).
23. L. R. Solman, *J. Photogr. Sci.* ISSN: 0022-3638, **18**, 179(1970).
24. L. R. Solman and G. C. Farnell, *J. Photogr. Sci.* ISSN: 0022-3638, **21**, 78(1973).
25. S. H. Kong, *J. Imaging Sci. Technol.* ISSN: 1062-3701, **49,** 348 (2005); *IS&Ts AgX 2004: The International Symposium on Silver Halide Technology*, (IS&T, Springfield, VA, 2004), p. 32.